Structure and cation distribution of $(Mn_{0.5}Zn_{0.5})Fe_2O_4$ thin films on $SrTiO_3(001)$

M. Welke, K. Brachwitz, M. Lorenz, M. Grundmann, K.-M. Schindler, A. Chassé, and R. Denecke

Citation: Journal of Applied Physics **121**, 225305 (2017); doi: 10.1063/1.4985175

View online: https://doi.org/10.1063/1.4985175

View Table of Contents: http://aip.scitation.org/toc/jap/121/22

Published by the American Institute of Physics

Structure and cation distribution of $(Mn_{0.5}Zn_{0.5})Fe_2O_4$ thin films on $SrTiO_3(001)$

M. Welke,[1] K. Brachwitz,[2] M. Lorenz,[2] M. Grundmann,[2] K.-M. Schindler,[3] A. Chassé,[3] and R. Denecke[1]
[1]*Wilhelm-Ostwald-Institut für Physikalische und Theoretische Chemie, Universität Leipzig, Linnéstraße 2, 04103 Leipzig, Germany*
[2]*Felix-Bloch-Institut für Festkörperphysik, Universität Leipzig, Linnéstraße 5, 04103 Leipzig, Germany*
[3]*Institut für Physik, Martin-Luther-Universität Halle-Wittenberg, Von-Danckelmann-Platz 3, 06120 Halle, Germany*

(Received 5 January 2017; accepted 25 May 2017; published online 12 June 2017)

A comprehensive study on growth of ferrimagnetic manganese zinc ferrite ($Mn_{0.5}Zn_{0.5}Fe_2O_4$) films on single crystalline strontium titanate(001) ($SrTiO_3$) substrates was carried out. Under the optimized conditions, a thin film with a layer thickness of 200 nm was deposited, and the structural properties were investigated. Contrary to data published in literature, no buffer layer was necessary to achieve epitaxial growth of a poorly lattice-matched layer. This was confirmed for $Mn_{0.5}Zn_{0.5}Fe_2O_4(001)$ on $SrTiO_3(001)$ by x-ray diffraction and the adjoined phi scans, which also revealed a lattice compression of 1.2% of the manganese zinc ferrite film in the *out-of-plane* direction. Using x-ray photoelectron spectroscopy, the near surface stoichiometry of the film could be shown to agree with the intended one within the uncertainty of the method. X-ray absorption spectroscopy showed an electronic structure close to that published for bulk samples. Additional x-ray magnetic circular dichroism investigations were performed to answer detailed structural questions by a comparison of experimental data with the calculated ones. The calculations took into account ion sites (tetrahedral vs. octahedral coordination) as well as the charge of Fe ions (Fe^{2+} vs. Fe^{3+}). Contrary to the expectation for a perfect normal spinel that only Fe^{3+} ions are present in octahedral sites, hints regarding the presence of additional Fe^{2+} in octahedral sites as well as Fe^{3+} ions in tetrahedral sites have been obtained. Altogether, the layer could be shown to be mostly in a normal spinel configuration. *Published by AIP Publishing.* [http://dx.doi.org/10.1063/1.4985175]

I. INTRODUCTION

Within the last two decades particular interest in ferrites and layered structures containing ferrites has developed.[1–11] As a matter of fact, ferrites prepared on perovskite-type or even spinel-type materials are very promising regarding structural and magnetic properties for applications as insulating magnetic barriers in magnetic tunnel junctions, as spin filters, or as magnetoelectric random access memory (MERAM) devices. For ferrite films grown on $SrTiO_3$, it has been claimed that good crystallinity along with good magnetic properties can only be achieved by using buffer layers such as $CoCr_2O_4$, $NiMn_2O_4$, or $MgAl_2O_4$.[5–7] The intention of these buffer layers is to prevent the diffusion of titanium into the layer[7] and to accommodate the lattice mismatch between the substrate and the layer which can be up to 10%. For $CoFe_2O_4$ and $NiFe_2O_4$, detailed studies about the growth with and without buffer layers on perovskites have been carried out.[12–14] It has to be mentioned that these two ferrites crystalize in an inverse spinel configuration in contrast to the $Mn_{1-x}Zn_xFe_2O_4$ studied here. A detailed review about thin ferrite films has been given by Suzuki in 2001.[11] Because of the lattice mismatch and the possible diffusion of titanium into the layer, the magnetic properties of the layer are reported to differ from the bulk properties.[6,9,15–19] Nevertheless, it was still possible to grow layers directly on $SrTiO_3$ without such buffer layers although the layers exhibited lattice parameters pointing to a large strain, which might be the reason of the variations in the films. Additionally, ferrites grown without buffer layers have shown magnetic properties, which makes them interesting candidates for various applications.[2–4,6,9,15–18]

One of the notably interesting ferrites for such layer systems is the mixed manganese zinc ferrite ($Mn_{1-x}Zn_xFe_2O_4$), one of the so-called soft magnetic power ferrites.[1] Bulk $Mn_{0.5}Zn_{0.5}Fe_2O_4$ has similar geometric properties as normal spinel-type $ZnFe_2O_4$ and partially inverse spinel-type $MnFe_2O_4$. In fact, all ferrites have lattice constants within the same range from 8.4 Å to 8.5 Å.[17,20–23] However, the magnetic properties differ due to different spinel type configurations as well as different elements involved. Furthermore, in thin films, $ZnFe_2O_4$ is shown to be ferrimagnetic due to A-B cation exchange in spinel AB_2O_4 and oxygen vacancies making it partially inverse contrary to bulk properties where it is found to be a complete normal spinel.[15–17,21,24] The usage of normal spinel type $Mn_{0.5}Zn_{0.5}Fe_2O_4$ is a part of the investigations regarding ferrites with a composition of $Mn_{1-x}Zn_xFe_2O_4$, some of which have been published already.[9,15–18,23,25] $Mn_{0.5}Zn_{0.5}Fe_2O_4$ can be understood as another spinel-type structure with intrinsic magnetic properties in bulk and thin films contrary to antiferromagnetic bulk $ZnFe_2O_4$, which exhibits no net magnetization in its ideal structure. On the other hand, bulk $MnFe_2O_4$ is magnetically very soft, and has a very low coercive field.[1] For

$Mn_{0.5}Zn_{0.5}Fe_2O_4$, soft magnetic behavior with a higher coercive field compared to pure $MnFe_2O_4$ has been shown making it more interesting for possible applications.[17,26–30]

In this paper, a preparative study regarding the structural aspects of a 200 nm thick $Mn_{0.5}Zn_{0.5}Fe_2O_4$ layer on perovskite-type $SrTiO_3(001)$ is reported. The lattice mismatch of $SrTiO_3$ and $(Mn_{1-x}Zn_xFe_2O_4)$ is up to 9% depending on the composition of manganese zinc ferrite. Nevertheless, a complete growth study using different growth conditions regarding substrate temperature (500 to 1000 K), oxygen partial pressure (6×10^{-5} to 0.1 mbar), and post-growth annealing has been carried out, while here the results of the optimized growth process are presented. As reported for $ZnFe_2O_4$ before, the preparation of the layer yielding the best composition as determined by x-ray photoelectron spectroscopy (XPS) as well as very sharp reflections in x-ray diffraction (XRD) has been chosen to be presented.[17,23] With the optimized growth conditions, it was possible to grow a crystalline, epitaxial layer as shown here.

Additionally, x-ray absorption spectra and related x-ray magnetic circular dichroism (XMCD) have been used to obtain the cation distribution in the $Mn_{0.5}Zn_{0.5}Fe_2O_4$ layer. A comparison between XMCD measurements and simulations using multiplet calculations was done to assign positions and valencies of cations in the layer.[31]

II. EXPERIMENTAL

A 200 nm thick film with the nominal composition $(Mn_{0.5}Zn_{0.5})Fe_2O_4$ (MZFO) was deposited from a bulk target of the same stoichiometry on a single crystalline $SrTiO_3(001)$ (STO) substrate employing pulsed laser deposition (PLD) using a KrF excimer laser with a wavelength of 248 nm. A total number of 30 000 pulses, a pulse energy of 600 mJ, and an energy density of 2 J/cm^2 yielded a layer with a thickness of 200 nm. During deposition, the STO substrate was heated to approximately 925 K in an O_2 atmosphere of 6×10^{-5} mbar. After deposition, the film has been heated at 750 K in an O_2 atmosphere of 6×10^{-5} mbar for 10 min. Due to their inertness, ferrite layers can be transferred between vacuum chambers through air and investigated by *ex-situ* measurements.[4] Using this possibility, the elemental composition of the layer was determined with x-ray photoelectron spectroscopy (XPS) using Al K_α radiation (1486.3 eV) on an *ESCALAB 220Xi* x-ray photoelectron spectrometer. Survey scans have been recorded with a pass energy of 50 eV and detail spectra with 10 eV. X-ray absorption spectroscopy (XAS) in total electron yield (TEY) mode was carried out at the UE56/2-PGM1 beamline at BESSY II with a resolution better than 0.2 eV. X-ray magnetic circular dichroism (XMCD) data were obtained from XAS spectra measured at the in-plane magnetized sample with circular polarized synchrotron radiation. Surface long range order was determined by low-energy electron diffraction (LEED) using a *SPECS* ErLEED 150. The smoothness of the surface was determined with an atomic force microscope (AFM), a *XE-150* from *Park Systems* using a silicon cantilever in non-contact mode. The crystallinity of the film was probed by XRD using a *Philips X'Pert* x-ray diffractometer. With Cu K_α radiation, a Bragg–Brentano goniometer with divergent/focussing beam optics was used. The azimuthal relationship between the layer and the substrate was obtained from XRD ϕ scans.

III. MULTIPLET CALCULATIONS

X-ray absorption spectra and, in particular, related XMCD are very sensitive to the local order in the film. Here, the $L_{2,3}$ edges of Mn and Fe in MZFO/STO(001) revealed additional information about the structure and cation distribution in the film. For the calculations the ligand-field multiplet (LFM) model was applied[32] using the program CTM4XAS.[33,34] Within this approximation, the transition metal ions of the film are considered as isolated ions surrounded by a distribution of charges, which mimic the solid around the ions. In the cubic case, the crystal field (or ligand field) is described by the cubic crystal field parameter 10 Dq, which is different for octahedral (O_h) and tetrahedral (T_d) complexes.

The most important parameters for all calculations are the valence of the cations and the crystal field parameter 10 Dq. It should be noted that compared to octahedral coordination, this parameter is smaller and reversed in sign for tetrahedral coordination. Different values for LORENTZIAN broadening have been used for the L_3 edge (0.3 eV) and the L_2 edge (0.5 eV). The GAUSSIAN broadening was set to be 0.4 eV at half-width half-maximum. Tetragonal distortions or charge transfer effects were neglected.

IV. RESULTS

After deposition of the film in a dedicated PLD chamber the sample was transferred through air to the *ESCALAB 220Xi* x-ray photoelectron spectrometer. In order to remove carbon containing contaminants adsorbed during transport, the sample was heated at 700 K in an oxygen atmosphere of 1×10^{-6} mbar O_2 for 30 min. Figure 1 shows the survey XPS spectrum as obtained after the treatment.

The inset shows the region of the C 1*s* photoemission line at around 285 eV. The signal of the C 1*s* line is at least 5 times smaller than that of the O 1*s* line considering both, intensity and cross-section. This residual amount could only be removed by sputtering, which would modify the thickness and stoichiometry of the layer.

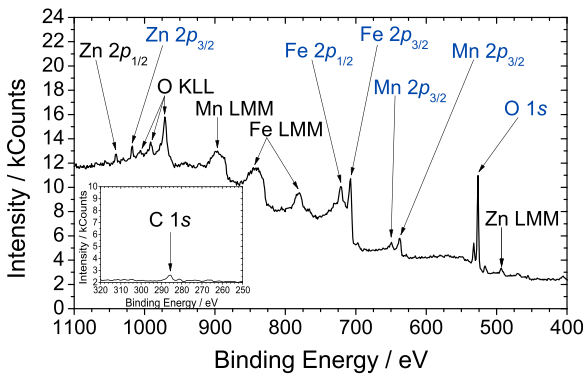

FIG. 1. Survey spectrum of the 200 nm thick $(Mn,Zn)Fe_2O_4$ on $SrTiO_3$ obtained after cleaning, with the lines labelled in blue analyzed quantitatively. The inset shows the spectrum around the C 1*s* line.

In addition to the survey scan of Fig. 1, detail scans of the lines labeled in blue (O 1*s*, Mn 2*p*, Fe 2*p*, and Zn 2*p*) were recorded in order to obtain the chemical environment of the elements as well as the near surface composition of the film. The spectral lines were fitted with a convolution of a GAUSSIAN and a LORENTZIAN function using the program UNIFIT 2014.[35] The background was fitted along with the lines using a SHIRLEY background function. The binding energies of the respective lines are listed in Table I. It has to be mentioned that only the main component of the Fe $2p_{3/2}$ signal is given there. For iron, two different peaks along with their satellites had to be used for a perfect fit (see Discussion). For manganese, the multiplet structure has been approximated by two components along with their satellites.

Due to the lack of a C 1*s* detail spectrum, O 1*s* was used as the binding energy reference with a value of 530.5 eV in order to calibrate the energy scale in accordance with the published data.[36] This type of referencing is necessary because of charging of the surface. Within typical uncertainties comparing absolute binding energy values obtained in different spectrometers and by different data analysis, there is a good agreement with the published binding energies. No additional peaks or shoulders were found, which could clearly identify other phases. The composition of the film has been determined from the atomic fractions obtained from fits of the detail scans. In translating the atomic fraction to composition, there is some ambiguity as different elements can be deliberately set to integer values. Taking into account the error bars of approximately 10%, the experimentally determined stoichiometry agrees quite well with the intended one ($Mn_{0.5}Zn_{0.5}Fe_2O_4$). In particular, the ratios of the metal components confirm the targeted stoichiometry. The oxygen content is less reliable due to the adsorbed species. Thus, we consider the resulting stoichiometry of $Mn_{0.43}Zn_{0.53}Fe_{1.9}O_4$ (using oxygen for normalization) as experimental proof of the targeted composition. Given the uncertainty in the oxygen content, both oxygen and cation vacancies cannot be excluded. The former might be related to the low applied oxygen pressure during PLD as it has been shown before (see Refs. 17, 23, and 36). The latter are also well known to exist in oxidic materials such as γ-Fe_2O_3.[37,38] It has to be mentioned that XPS only probes the near surface region within a few nm. Regarding the diffusion of titanium into the bulk of the layer, as reported for $CoFe_2O_4$ on $SrTiO_3$,[7] only long-range diffusion could be excluded because of the limited information depth of XPS and the thickness of the layer.

TABLE I. Binding energies of the main maxima of the peaks used in quantification compared to literature.[36]

Core-level	Experiment /eV	Reference /eV
O 1*s*	530.5	530.5
Mn $2p_{3/2}$	640.8	641.3
Fe $2p_{3/2}$	711.1	711.4
Zn $2p_{3/2}$	1022.5	1022.0

As a complementary method to XPS, additional x-ray absorption spectra at the O *K* edge, Mn *L* edge, and Fe *L* edge were recorded. Here, only the Mn *L* edge and the Fe *L* edge are shown in Figs. 2(a) and 2(b) (marked as the sum curve). The spectra were recorded in the total electron yield (TEY) mode. Therefore, the layer thickness of 200 nm prevented the detection of any signal from the $SrTiO_3$ substrate.

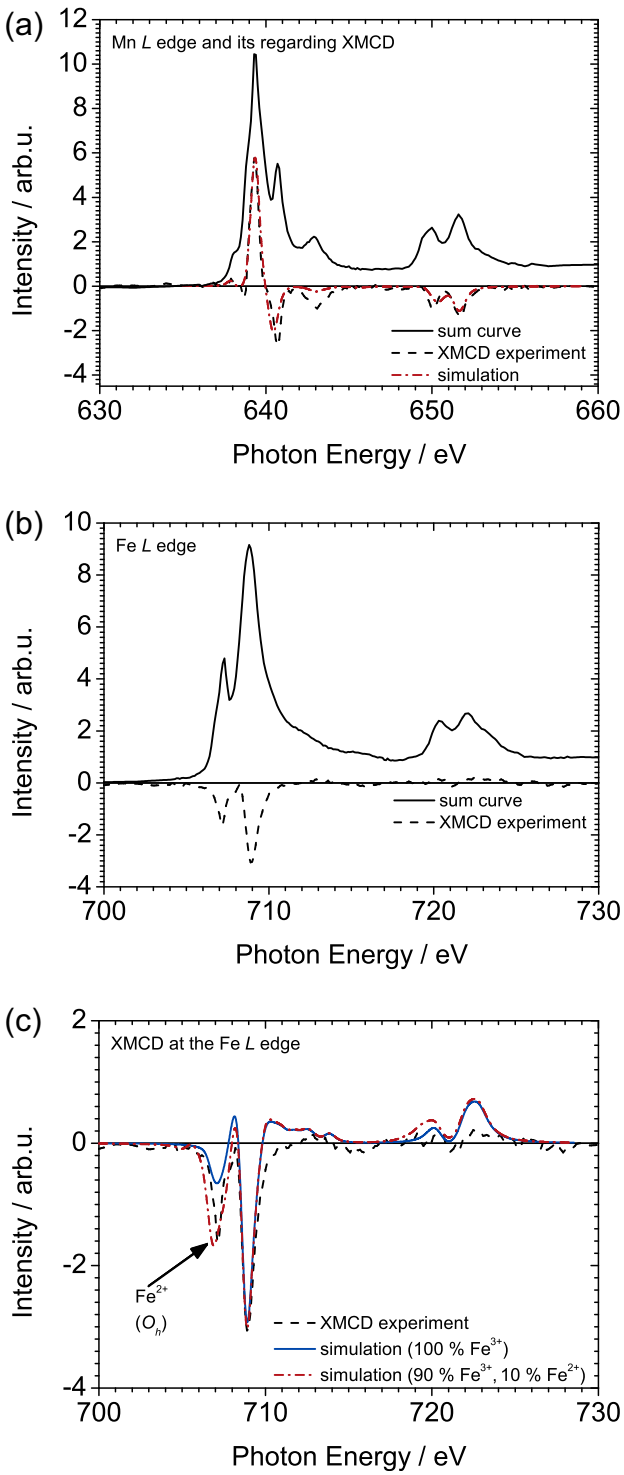

FIG. 2. X-ray absorption spectra and their subsequent XMCD with the adjoined theoretical calculation of the 200 nm thick $(Mn,Zn)Fe_2O_4$ layer on $SrTiO_3$ with (a) Mn *L* edge, (b) Fe *L* edge and, (c) simulation of the XMCD at the Fe *L* edge.

Both XAS spectra were normalized to an edge jump of one. The XAS spectra obtained for the Mn *L* edge and the Fe *L* edge correspond very well to those published in literature for bulk and thin film ferrites.[4,18,25,27,39,40] In order to obtain more detailed information, XMCD spectra have been measured at both edges. These data are also presented in Fig. 2 together with results of simulations, in particular, for the Fe *L* edge in Fig. 2(c).

LEED pattern images were recorded for the 200 nm ferrite film at an electron kinetic energy of 160 eV (data not shown here). The fourfold symmetry of the diffraction pattern, the orientation of the pattern, and the position of the diffraction spots correspond to the pattern from the underlying $SrTiO_3$ substrate. Integer order diffraction spots were of weak intensity and considerably broadened. No fractional order diffraction spots hinting to a superstructure were observed.

The roughness of the layer was determined from AFM images like the one in Fig. 3 where the maximum height difference is 12.6 nm [15 unit cells of $(Mn,Zn)Fe_2O_4$]. The RMS of the area shown has a value of 1.27 nm. Obviously, the layer is composed of well-oriented square crystallites, 300 nm in size.

In XRD, the $(Mn,Zn)Fe_2O_4$ layer shows well-defined peaks besides the ones of $SrTiO_3$, which could be assigned to crystal reflections named in Fig. 4(a). Only the reflections associated with a (001) surface could be found and show that the MZFO layer also exhibits the (001) surface plane, which corresponds to the $SrTiO_3$(001) substrate.

In addition to these findings, there are two additional reflections at 38° and 55° labeled by asterisks in Fig. 4(a) as they can be assigned to an impurity phase. This impurity phase could be assigned to $MnFeO_3$. On the other hand, no impurity phases of Fe_2O_3 or Mn_2O_3 are present, as found as a function of annealing temperature for the preparation of $(Mn,Zn)Fe_2O_4$ via another route.[41] Altogether, manganese zinc ferrite predominates the spectrum by 100 to 1 considering the logarithmic scale in Fig. 4(a). The calculated mean *out-of-plane* lattice constant of the $(Mn,Zn)Fe_2O_4$ film is 8.371 Å with a FWHM of the (004) peak of 0.15°, which results in a compression of 1.2% compared to the bulk value of 8.480 Å for $(Mn_{0.4}Zn_{0.6})Fe_2O_4$.[21] For $SrTiO_3$, the lattice constant is calculated to be 3.904 Å with a FWHM of 0.12° coinciding with the exact value given in literature.[42]

Additionally to these 2θ-ω scans, ϕ scans were obtained using the $SrTiO_3$(311) and $(Mn,Zn)Fe_2O_4$(511) reflections in order to reveal an *in-plane* epitaxial relationship of the parallel aligned lattice directions of $[001](Mn,Zn)Fe_2O_4 \parallel [001]SrTiO_3$ [see Fig. 4(b)].

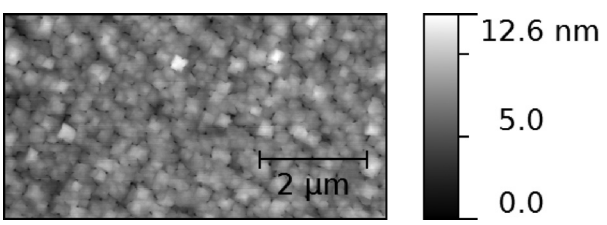

FIG. 3. AFM image of the 200 nm $(Mn,Zn)Fe_2O_4$ film on $SrTiO_3$.

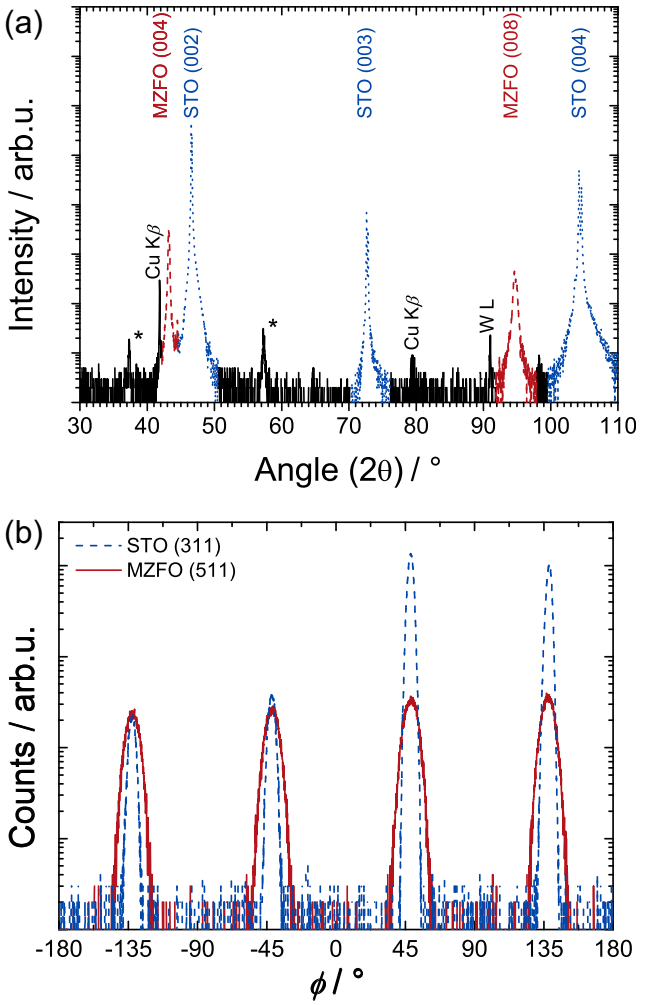

FIG. 4. (a) XRD of the layer system of $(Mn,Zn)Fe_2O_4$ on $SrTiO_3$ with additional spectral lines from Cu K_β, W L_α, and an impurity phase of $MnFeO_3$ labeled as * as well as (b) the XRD ϕ scan using $SrTiO_3$(311) and $(Mn,Zn)Fe_2O_4$(511).

V. DISCUSSION

Utilizing the experimental results together with theoretical calculations of the XAS data, details of the structure of the $(Mn_{0.5}Zn_{0.5})Fe_2O_4$ layer can be derived.

Comparing the XPS core-level binding energy of the Mn2$p_{3/2}$ emission line at 640.8 eV with published ones suggests Mn^{2+} coordinated by oxygen.[43] Higher oxidation states of manganese are very unlikely, since they would exhibit much higher binding energies. For example, Mn^{4+} in MnO_2 exhibits a core-level binding energy of 641.9 eV. Nevertheless, Mn^{3+} with its reported binding energy at 641.2 eV (Ref. 43) would be a possible candidate in light of the $MnFeO_3$ impurity phase detected in XRD. However, the peak fit did not reveal such a component as it might be below the detection limit of XPS. Furthermore, a Zn environment of the Mn could also be the origin of this binding energy deviating from metallic Mn as this was discussed before.[36]

As it can be seen in Fig. 5, two peaks concerning Fe^{3+} ions as well as two satellite peaks to these two main peaks are needed for a good match with the fitting procedure. In order to explain different binding energies of equally charged Fe^{3+} ions the chemical surrounding of these ions

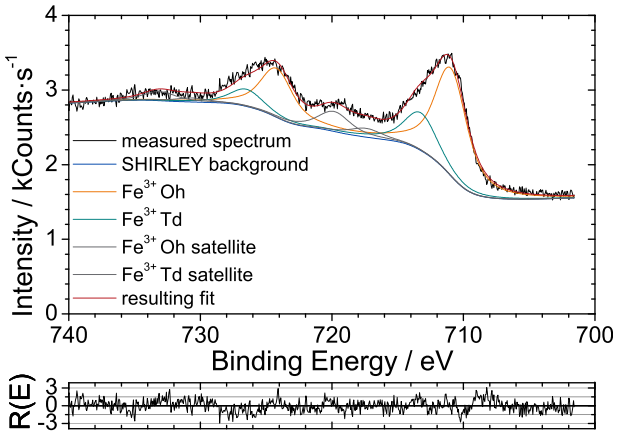

FIG. 5. Detail spectrum with the resulting fit of the Fe 2*p* core level.

has to be considered. In fact, the main Fe $2p_{3/2}$ photoemission line with a binding energy of 711.1 eV indicates Fe^{3+} coordinated by oxygen. This statement is endorsed by comparing this binding energy to Fe^{3+} in Fe_3O_4.[44,45] At 713.5 eV, an additional peak is needed in order to obtain a good fit of the measured spectrum. This additional peak can be related to Fe^{3+} as well. In a perfectly ordered normal spinel, all Fe^{3+} ions are situated in octahedral sites only. Then, only one binding energy is observed. For Fe^{3+} ions in tetrahedral sites a higher core-level binding energy is expected due to the ligand field splitting. For $CoFe_2O_4$ on $BaTiO_3$, such a behavior of the binding energies has been described before.[14] Therefore, different lattice positions of Fe^{3+} ions have been made responsible for the splitting in binding energies of the main peak. $CoFe_2O_4$ crystallizes in an inverse spinel structure so that a very high portion of Fe^{3+} in tetrahedral sites has been observed. As seen in Fig. 5, the $(Mn_{0.5}Zn_{0.5})Fe_2O_4$ layer also exhibits both Fe^{3+} coordinations. In this case, the occupation of tetrahedral sites is significantly smaller (a ratio of 3:1 between octahedral and tetrahedral sites) showing that only a quarter of the Fe^{3+} ions is occupying the site contrary to the normal spinel structure. This ratio could be confirmed using a simulation of the XMCD data of iron as discussed below. As a matter of fact, the peak ratio of inverse spinel-type $CoFe_2O_4$ is reversed to the ones observed in this study.[14]

Since XAS is considered to be more sensitive to oxidation states than XPS,[46] those results are discussed now. Previously, the Mn *K* and Fe *K* edges have been used to describe the distribution of cations.[22,47] Nevertheless, the *L* edges can be obtained easier by experimental means. The observation that the general structure of the XAS spectra shown in Fig. 2 resembles those published for a wide range of compositions on different substrates calls for a closer look at the absorption data.

In particular, XMCD data are very sensitive regarding small changes of oxidation states and chemical environment. In Fig. 2, the XMCD of the Mn *L* edge is very well described by a simulation assuming Mn^{2+} in tetrahedral sites only [see Fig. 2(a)]. The XMCD of the Fe *L* edge cannot be reproduced assuming Fe^{3+} in octahedral sites only as expected for a normal spinel structure. In agreement to the XPS results some part of the Fe^{3+} ions has to be situated in tetrahedral sites as well. In this case, the best agreement between experiment and theory has again been found for a ratio 3:1 concerning the occupation of Oh and Td sites [see Fig. 2(c)]. The simulations were done using 1.4 eV and −0.6 eV for the parameter 10 Dq, respectively. An essential improvement (especially for the low energy negative contribution in XMCD) is achieved assuming 10% of Fe^{2+} ions in octahedral positions [see Fig. 2(c)]. This is underlined by a very small shoulder at 705 eV in the absorption spectrum. Reconsidering the XPS data, these findings can also be supported there.

However, Fe^{2+} ions have a considerably low electron binding energy in Fe_3O_4 so that they cannot be assigned with any of the two main peaks in the Fe $2p_{3/2}$ of Fig. 5.[44,45] A closer look to the Fe detail spectrum reveals deviation in the residuum at a binding energy of ≈710 eV. This binding energy corresponds well to the Fe^{2+} contribution in the spectrum of Fe_3O_4. Therefore, this additional contribution indicates that besides Fe^{3+} there may also be a small amount of Fe^{2+}.[44,45] Due to the small difference in binding energies of Fe^{2+} and Fe^{3+} in octahedral sites it is not possible to distinguish these two contributions to the full extent. Thus, a quantification of the amount of Fe^{2+} is not possible. Therefore, no value is given here. Nevertheless, these findings correspond to the distinct shoulder found in the Fe *L* edge absorption spectrum. However, it is possible that there are less Fe^{2+} at the surface measured by XPS as compared to more bulk sensitive XAS measurement.

This additional Fe^{2+} could result from intrinsic defects of the manganese zinc ferrite layer. For example, oxygen vacancies would allow the presence of Fe^{2+} ions in order to have charge neutrality within the layer. However, early calculations reported such contributions even for the ideal structure[48,49] while others connected them with defects, especially in nanostructured samples[28] or related to annealing temperature.[30] Additionally, it is possible that a small portion of Fe_3O_4 has formed as well, which could not be distinguished by the experimental means used for analysis. Fe_3O_4 exhibits such Fe^{2+} in octahedral sites, which could contribute to the signal observed in Fig. 2(c). On the other hand, a higher portion of Fe^{3+} in tetrahedral sites would then be expected which has not been observed in the XMCD spectra.

The Zn $2p_{3/2}$ photoemission line has a binding energy of 1022.5 eV, indicating oxygen coordinated Zn^{2+} in good agreement with previous publications.[44,45] Finally, it can be stated that XPS showed no traces of metallic parts or other unexpected oxidation states.

The LEED diffraction pattern of the $(Mn,Zn)Fe_2O_4$ layer exhibits a fourfold symmetry. Orientation of the pattern and position of the integral order diffraction spots correspond well to the pattern of the underlying $SrTiO_3$ substrate. This indicates epitaxial growth as previously found for isostructural Fe_3O_4 on $BaTiO_3$[50] and is in agreement with the XRD investigations as discussed below. No fractional order diffraction spots have been observed. However, the presence of a superstructure cannot completely be ruled out, because the intensities of the LEED pattern were quite low on a high

background and the spots were considerably broadened. The size of the crystallites in the film (AFM images from above: 300 nm) is well beyond the transfer width of the LEED optics and can therefore be ruled out as a reason for the broadening. Therefore, three other mechanisms remain regarding the broadening of the diffraction spots. First, a surface roughness of 15 unit cells (determined from the peak-to-tail roughness of 12.6 nm from the AFM image in Fig. 3 and the lattice constant of 8.371 Å) can be connected to small terraces. However, a similar spot broadening has been observed with a Fe_3O_4 film on $BaTiO_3$,[50] although the film had a much smoother surface. Therefore, the next two reasons are more likely: in XPS, residual carbon has been observed, which causes disorder at the surface. Finally, the low conductivity of substrate and film can cause substantial charging.

In XRD a parallel orientation of the crystallites could be concluded for the whole layer as well as there are manganese zinc ferrite reflections corresponding to the (001) oriented STO substrate only. This leaves the layer to be (001)-textured only. On the other hand, an impurity phase has been found that can form during PLD. In fact, this impurity phase could be assigned to $MnFeO_3$ with a fraction of less than 1% of the whole layer. Additionally, small exudations of other ferrite materials such as Fe_3O_4 could be possible that cannot be distinguished using XRD. For the manganese zinc ferrite layer, a compression of 1.2% results in a mean *out-of-plane* lattice constant of 8.371 Å, while bulk $(Mn_{0.5}Zn_{0.5})Fe_2O_4$ is in between 8.48 Å for $(Mn_{0.4}Zn_{0.6})Fe_2O_4$ and 8.50 Å for $(Mn_{0.6}Zn_{0.4})Fe_2O_4$.[20,21] Even the experimental lattice constant for $(Mn_{0.8}Zn_{0.2})Fe_2O_4$ has a value of 8.50 Å (Ref. 22) so that there are only small changes for this structure type. Furthermore, the lattice constant of the substrate can be assigned to a value of 3.904 Å in agreement with published data.[42] However, the resulting lattice mismatch (by taking the doubled lattice parameter of $SrTiO_3$ as a reference for the calculation) between 7% and 9% for a cubic lattice or an expanded *in-plane* lattice constant, respectively, would contradict the possibility of epitaxial growth of such a layer, which was one of the aims of the work presented. Angular dependent measurements of the reflections of $SrTiO_3$(311) and (Mn,Zn)Fe_2O_4(511) were carried out showing only parallel orientations of the layer to the substrate, which is similar to the behavior of $ZnFe_2O_4$ on $SrTiO_3$.[17,23,24] It can be speculated that this epitaxial growth is possible due to a large dislocation density at the interface that subsides throughout the film and causes a gradual change of the lattice constant within a few layers.

VI. CONCLUSION

In this paper the structure of a 200 nm thick layer of (Mn,Zn)Fe_2O_4 on $SrTiO_3$ has been characterized using XPS, XAS, XMCD, LEED, AFM, and XRD. A growth study varying the substrate temperature as well as the oxygen partial pressure during PLD has been carried out where optimized growth conditions could be derived with a substrate temperature of 1000 K in a 6×10^{-5} mbar O_2 atmosphere (see Refs. 17 and 23 for comparable results). After deposition of the different layers they have been examined using XPS and XRD. Combining the results of both methods, the optimized growth conditions have been derived for the preparation of the presented 200 nm thick manganese zinc ferrite layer on strontium titanate which has been analyzed in further detail. By optimizing the growth conditions, epitaxial growth, very good crystallinity and the intended composition could be obtained without a buffer layer contrary to previous claims.[5–7] In detail, the epitaxial relation was determined from XRD and LEED as [001](Mn,Zn)Fe_2O_4 || [001]$SrTiO_3$. The quantitative analysis of XPS photoemission lines of that layer has revealed a near surface composition of $Mn_{0.43}Zn_{0.53}Fe_{1.9}O_4$, which is in good agreement with the intended composition of $Mn_{0.5}Zn_{0.5}Fe_2O_4$ showing the high quality of the surface of the layer. The analysis of XMCD spectra at the *L* edges of Fe and Mn revealed the presence of additional Fe^{2+} ions in octahedral sites. Nevertheless, the layer seems to be mostly in a normal spinel configuration as there are only 25% Fe^{3+} in tetrahedral sites.

However, it is possible that the composition in larger depths deviates from the calculated surface composition due to segregation effects. AFM shows that the film consists of connected square shaped islands with preferential alignment of the island edges. The high structural quality and its reproducibility make it a prime candidate for investigating its magnetic properties that are presented in detail elsewhere.[51]

ACKNOWLEDGMENTS

Financial support from the DFG through the framework of the SFB 762 "Functionality of Oxide Interfaces" is gratefully acknowledged. The authors thank W. Mahler and B. Zada at BESSY II for technical support during beamtimes, Gabriele Ramm for producing the PLD targets, and all members of the SFB 762 for mutual technical support and stimulating scientific discussions.

[1]D. Stoppels, J. Magn. Magn. Mater. **160**, 323 (1996).
[2]G. E. Sterbinsky, B. W. Wessels, J.-W. Kim, E. Karaptetrova, P. J. Ryan, and D. J. Kaevney, Appl. Phys. Lett. **96**, 092510 (2010).
[3]Y. Z. Chen, J. R. Sun, Y. N. Han, X. Y. Xie, J. Shen, C. B. Rong, S. L. He, and B. G. Shen, J. Appl. Phys. **103**, 07D703 (2008).
[4]E. Arenholz, G. van der Laan, R. Chopdekar, and Y. Suzuki, Phys. Rev. B **74**, 094407 (2006).
[5]Y. Suzuki, R. B. van Dover, E. M. Gyorgy, J. M. Phillips, V. Korenivski, D. J. Werder, C. H. Chen, R. J. Felder, R. J. Cava, J. J. Krajewski, and W. F. J. Peck, J. Appl. Phys. **79**, 5923 (1996).
[6]Y. Suzuki, R. B. van Dover, E. M. Gyorgy, J. M. Phillips, V. Korenivski, D. J. Werder, C. H. Chen, R. J. Cava, J. J. Krajewski, W. F. Peck, and K. B. Do, Appl. Phys. Lett. **68**, 714 (1996).
[7]J. M. Rebled, M. Foerster, S. Estradé, F. Rigato, C. Kanamadi, F. Sánchez, F. Peiró, and J. Fontcuberta, Phys. Chem. Chem. Phys. **15**, 18274 (2013).
[8]C. A. F. Vaz, J. Hoffmann, A.-B. Posadas, and C. H. Ahn, Appl. Phys. Lett. **94**, 022504 (2009).
[9]M. Niranjan, J. Velev, C.-G. Duan, S. Jaswal, and E. Tsymbal, Phys. Rev. B **78**, 104405 (2008).
[10]J. Gräfe, M. Welke, F. Bern, M. Ziese, and R. Denecke, J. Magn. Magn. Mater. **339**, 84 (2013).
[11]Y. Suzuki, Annu. Rev. Mater. Res. **31**, 265 (2001).
[12]C. Klewe, M. Meinert, A. Boehnke, K. Kuepper, E. Arenholz, A. Gupta, J.-M. Schmalhorst, T. Kuschel, and G. Reiss, J. Appl. Phys. **115**, 123903 (2014).

[13]T. Niizeki, Y. Utsumi, R. Aoyama, H. Yanagihara, J.-i. Inoue, Y. Yamasaki, H. Nakao, K. Koike, and E. Kita, Appl. Phys. Lett. **103**, 162407 (2013).
[14]T. Aghavnian, J.-B. Moussy, D. Stanescu, R. Belkhou, N. Jedrecy, H. Magnan, P. Ohresser, M.-A. Arrio, P. Sainctavit, and A. Barbier, J. Electron Spectrosc. Relat. Phenom **202**, 16 (2015).
[15]C. E. Rodríguez Torres, F. Golmar, M. Ziese, P. Esquinazi, and S. P. Heluani, Phys. Rev. B **84**, 064404 (2011).
[16]C. E. Rodríguez Torres, G. A. Pasquevich, P. M. Zélis, F. Golmar, S. P. Heluani, S. K. Nayak, W. A. Adeagbo, W. Hergert, M. Hoffmann, A. Ernst, P. Esquinazi, and S. J. Stewart, Phys. Rev. B **89**, 104411 (2014).
[17]M. Lorenz, M. Brandt, K. Mexner, K. Brachwitz, M. Ziese, P. Esquinazi, H. Hochmuth, and M. Grundmann, Phys. Status Solidi RRL **5**, 438 (2011).
[18]U. S. Alaan, F. J. Wong, A. J. Grutter, J. M. Iwata-Harms, V. V. Mehta, E. Arenholz, and Y. Suzuki, J. Appl. Phys. **111**, 07A337 (2012).
[19]S. Zhou, K. Potzger, D. Bürger, K. Kuepper, M. Helm, J. Fassbender, and H. Schmidt, J. Nucl. Instrum. Met. Phys. B **267**, 1620 (2009).
[20]M. El Guendouzi, K. Sbai, P. Perriat, and B. Gillot, Mater. Chem. Phys. **25**, 429 (1990).
[21]U. König and G. Chol, J. Appl. Cryst. **1**, 124 (1968).
[22]S. Sakurai, S. Sasaki, M. Okube, H. Ohara, and T. Toyoda, Physica B **403**, 3589 (2008).
[23]K. Brachwitz, T. Böntgen, M. Lorenz, and M. Grundmann, Appl. Phys. Lett. **102**, 172104 (2013).
[24]K. Brachwitz, see http://nbn-resolving.de/urn:nbn:de:bsz:15-qucosa-141251 for "Defekt-induzierte Leitungsmechanismen und magnetische Eigenschaften spinellartiger Ferrite," Ph.D. thesis (Universität Leipzig, 2014).
[25]J. S. Bettinger, C. Piamonteze, R. V. Chopdekar, M. Liberati, E. Arenholz, and Y. Suzuki, Phys. Rev. B **80**, 140413(R) (2009).
[26]S. Imada, A. Kimura, T. Muro, S. Suga, and T. Miyahara, J. Electron Spectrosc. Relat. Phenom. **88–91**, 195 (1998).
[27]S. Suga and S. Imada, J. Electron Spectrosc. Relat. Phenom. **92**, 1 (1998).
[28]E. Veena Gopalan, K. A. Malini, D. Sakthi Kumar, Y. Yoshida, I. A. Al-Omari, S. Saravanan, and M. R. Anantharaman, J. Phys.: Condens. Matter **21**, 146006 (2009).
[29]K. C. Verma, V. P. Singh, M. Ram, J. Shah, and R. Kotnala, J. Magn. Magn. Mater. **323**, 3271 (2011).
[30]C. M. Williams, D. B. Chrisey, P. Lubitz, K. S. Grabowski, and C. M. Cotell, J. Appl. Phys. **75**, 1676 (1994).
[31]J. Crocombette, M. Pollak, F. Jollet, N. Thromat, and M. Gautier-Soyer, Phys. Rev. B **52**, 3143 (1995).
[32]F. M. F. de Groot, J. C. Fuggle, B. T. Thole, and G. A. Sawatzky, Phys. Rev. B **42**, 5459 (1990).
[33]E. Stavitski and F. de Groot, Micron **41**, 687 (2010).
[34]H. Ikeno, F. M. F. de Groot, E. Stavitski, and I. Tanaka, J. Phys.: Condens. Matter **21**, 104208 (2009).
[35]R. Hesse, see http://www.uni-leipzig.de/unifit/ for "Unifit 2014".
[36]P. A. Atanasov, M. E. Koleva, R. I. Tomov, and V. I. Krastev, J. Mater. Sci.: Mater. Electron. **10**, 295 (1999).
[37]C. J. Serna and M. P. Morales, Surf. Colloid Sci. **17**, 27 (2004).
[38]R. Grau-Crespo, A. Y. Al-Baitai, I. Saadoune, and N. H. De Leeuw, J. Phys.: Condens. Matter **22**, 255401 (2010).
[39]M. Magnuson, L.-C. Duda, S. Butorin, P. Kuiper, and J. Nordgren, Phys. Rev. B **74**, 172409 (2006).
[40]J.-S. Kang, G. Kim, H. J. Lee, D. H. Kim, H. S. Kim, J. H. Shim, S. Lee, H. Lee, J.-Y. Kim, B. H. Kim, and B. I. Min, Phys. Rev. B **77**, 035121 (2008).
[41]P. Hu, H. Yang, D. Pan, H. Wang, J. Tian, S. Zhang, X. Wang, and A. A. Volinsky, J. Magn. Magn. Mater. **322**, 173 (2010).
[42]Y. A. Abramov, V. G. Tsirelson, V. E. Zavodnik, S. A. Ivanov, and I. D. Brown, Acta. Cryst. B **51**, 942 (1995).
[43]A. J. Nelson, J. G. Reynolds, and J. W. Roos, J. Vac. Sci. Technol. A **18**, 1072 (2000).
[44]T. Fujii, F. M. F. de Groot, G. A. Sawatzky, F. C. Voogt, T. Hibma, and K. Okada, Phys. Rev. B **59**, 3195 (1999).
[45]S. Krasnikov, A. Vinogradov, K.-H. Hallmeier, R. Höhne, M. Ziese, P. Esquinazi, T. Chassé, and R. Szargan, Mater. Sci. Eng., B **109**, 207 (2004).
[46]J. Stöhr and G. Ertl, eds., *NEXAFS Spectroscopy* (Springer-Verlag, 1992).
[47]B. Jeyadevan, K. Tohji, K. Nakatsuka, and A. Narayanasamy, J. Magn. Magn. Mater. **217**, 99 (2000).
[48]J. B. Goodenough, W. Gräper, F. Holtzberg, D. L. Huber, R. A. Lefever, J. M. Longo, T. R. McGuire, and S. Methfessel, *Landolt-Börnstein New Series III/4b: Magnetic and Other Properties of Oxides and Related Compounds* (Springer-Verlag, Berlin, Heidelberg, New York, 1970), p. 126.
[49]Y. G. Saksonov and V. A. Somenkov, Fiz. Met. Metalloved. **18**, 853 (1964).
[50]V. H. Babu, R. K. Govind, K.-M. Schindler, M. Welke, and R. Denecke, J. Appl. Phys. **114**, 113901 (2013).
[51]M. Welke, "Magnetic and electronic structure of thin ferro- and ferrimagnetic layers on perovskite-like substrates – Studies towards multiferroic layer systems," Ph.D. thesis (Universität Leipzig, 2016).